JACS
JOURNAL OF THE AMERICAN CHEMICAL SOCIETY
pubs.acs.org/JACS
Article

A Cyclometalated Gold(III) Complex Targets Mitochondrial VDAC1 to Drive Immunometabolic Reprogramming in Cancer

Sean T. Gilpatrick, Jong Hyun Kim, Sarayu Bhogoju, Neeraj Kapur, Udara Munugoda, Jovita Daraezinwa, Sean Parkin, Terrence A. Barrett, Christine F. Brainson, Daniel R. Plaugher, and Samuel G. Awuah*

Cite This: https://doi.org/10.1021/jacs.6c00003
Read Online
ACCESS | Metrics & More | Article Recommendations | Supporting Information

ABSTRACT: Chemotherapeutic agents can modulate inflammatory and immune pathways in cancer, yet the molecular mechanisms linking small-molecule target engagement to immune remodeling remain poorly defined. Here, we identify the mitochondrial voltage-dependent anion channel 1 (VDAC1) as a direct target of a cyclometalated gold(III) bisphosphine complex (AuPhos), establishing a mechanistic connection between VDAC1 engagement and immunometabolic reprogramming in tumor cells. Using complementary chemical proteomics, cellular thermal shift assays, intact mass spectrometry, and top-down proteomics, we demonstrate that AuPhos covalently engages and stabilizes VDAC1 at cysteine 232. In cancer cells, VDAC1 targeting by AuPhos disrupts mitochondrial metabolic homeostasis, including selective downregulation of respiratory electron transport chain transcripts, and induces intrinsic inflammatory signaling characterized by cytokine and chemokine expression (IL-6, IL-18, IL-8, IL-1β, and CXCL10). Notably, pro-inflammatory transcriptional responses are selectively induced in cancer cells, while mitochondrial metabolic responses occur in both cell-type-dependent directions. Beyond tumor cell−intrinsic effects, AuPhos enhances peripheral blood mononuclear cell (PBMC) activation and augments immune cell-mediated killing of cancer cells. Together, these findings identify VDAC1 as a previously unrecognized target of gold(III) complexes and establish AuPhos as a chemical probe and prototype for redox-active, metal-based agents capable of coupling mitochondrial targeting to immunometabolic remodeling in cancer with implications for several pathologies.

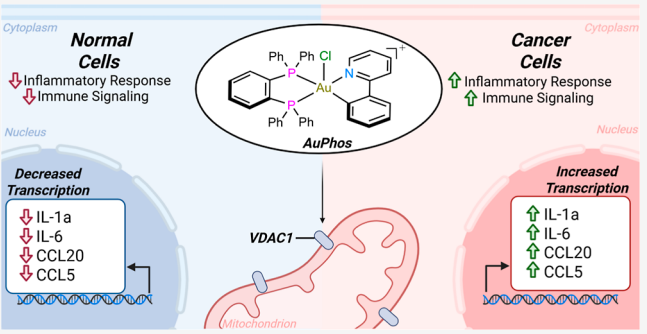

INTRODUCTION

The tumor microenvironment is shaped not only by intrinsic oncogenic signaling but also by metabolic and immunological cues that dictate therapeutic responses.[1] While immune checkpoint inhibitors have transformed cancer therapy,[2] strategies that induce cancer cell-biased inflammatory reprogramming through defined molecular mechanisms remain underdeveloped. In particular, exploiting metabolic stress pathways to trigger context-dependent cytokine induction within cancer cells offers a promising approach to rewire immune signaling. Recent work suggests that targeted disruption of mitochondrial homeostasis can provoke immunogenic stress,[3] yet the link between mitochondrial gatekeeping and inflammatory transcriptional responses is not well characterized. Here, we report that a cyclometalated gold(III) bisphosphine complex (AuPhos) engages VDAC1, a mitochondrial outer membrane channel, to initiate metabolic dysfunction and selectively upregulate inflammatory cytokines and chemokines including IL-10, IL-4, IL-1α, and CXCL family members in tumor cells but not normal epithelial cells. This selective inflammatory reprogramming points to a new modality of immunometabolic intervention, where gold-based organometallic complexes can function as chemical triggers of tumor-localized immune activation via mitochondrial disruption.

The voltage-dependent ion channel 1 (VDAC1) is the most expressed isoform of the VDAC family of proteins.[4] VDAC1 is a key hub protein influencing cell energy and metabolism, due to its role as the facilitator of metabolite transport in and out of the mitochondria.[5] This implicates VDAC1 in numerous disease indications such as cancer,[6] Alzheimer's,[7] type 2 diabetes,[8] and ischemia-reperfusion injury.[9] As a result, massive efforts have been put forth to identify molecular scaffolds that target VDAC1. Early work by Stockwell and co-workers found that Erastin interacts with VDAC proteins in BJ-TERT/LT/ST/RAS^{V12} cells to induce oxidative cell death.[10] Later, work by Shoshan-Barmatz and co-workers identified ruthenium-based molecules, azido ruthenium (AzRu) and ruthenium red (RuR),

Received: January 1, 2026
Revised: May 22, 2026
Accepted: May 26, 2026

ACS Publications
© XXXX The Authors. Published by American Chemical Society

that bind VDAC1 at glutamate 73 (E73) to protect against cytochrome c release and cell death induced by overexpression of VDAC1.[11] Recently, Shoshan-Barmatz et al. developed the VBIT class of molecules that prevent VDAC oligomerization and inhibit apoptosis.[12] VBIT-4 and VBIT-12 protect against Alzheimer's disease pathology,[13] restores β cell function in type 2 diabetes,[14] ameliorate lupus-like symptoms in mice models of lupus,[15] and alleviate Ulcerative Colitis symptoms in dextran sulfate sodium-treated mice.[16] Whereas these examples demonstrate the vital role of VDAC1 in disease and cell function, there persists a need to fully elucidate the biological mechanisms dictated by VDAC modulation.

In recent years, gold (Au)-containing compounds have emerged as promising therapeutic agents toward the treatment of disease.[17] Work in the 20th century by Forestier and Sutton revealed the efficacy of gold salts and complexes toward the treatment of rheumatoid arthritis, a chronic inflammatory autoimmune disorder.[18,19] This resulted in FDA approval of the Au(I)-containing drug auranofin, for treatment of Rheumatoid arthritis.[18,20] Mechanistic studies show that auranofin can modulate inflammatory immune signaling through toll-like receptor 4 (TLR4)[21] and inhibition of NF-κB signaling.[22] Recently, much work has been put forth toward understanding the underlying mechanisms that afford gold complexes therapeutic efficacy. This has resulted in the design of gold complexes with novel structural scaffolds and unique biological mechanisms, including perturbation of mitochondria,[23] induction of endoplasmic reticulum stress,[24,25] and inhibition of the ubiquitin proteasome system (UPS).[26] Given the central role of mitochondrial hub proteins in orchestrating immunometabolic signaling, we investigated a series of cyclometalated Au(III) complexes bearing bisphosphine ligands (AuPhos) for their potential to inhibit tumor growth in vitro and in vivo.[27] Work by Mármol and co-workers in the design of an alkynyl gold(I) complex showed the ability for the molecule to induce necroptosis, a cell death pathway reliant on TNF-α and NF-κB signaling pathways.[28] Further work by Cheng et al. on *N*-heterocyclic carbene (NHC) gold complexes found that these organogold complexes are potent aryl hydrocarbon receptor (AHR) agonists, resulting in activation of TGFβ1 signaling and suppressing $CD4^+$ T-cell activation.[29] Sessler and colleagues also demonstrated that NHC−Au(I) complexes can induce immunogenic cell death by disrupting cellular antioxidant networks.[24,30] Despite the abundance of evidence showing the ability of gold complexes to modulate cellular processes involved in inflammatory-immune signaling pathways, there persists a gap in knowledge of the direct biomolecular interactions evoking these responses.

In contrast to Au(I), which typically adopts linear coordination geometries and preferentially engages highly nucleophilic soft donors such as selenocysteine residues,[31] cyclometalated Au(III) complexes provide a structurally rigid, square-planar scaffold with distinct electronic and coordination properties.[32] Stabilization by [C^N]-cyclometalating ligands and ancillary phosphines enhances resistance to reduction under physiological conditions while enabling tunable electrophilicity and ligand exchange behavior.[33,34] In this work, the resulting AuPhos scaffold exhibits a well-defined coordination environment and a reduction potential of approximately −0.5 V, consistent with electrochemical stability under biologically relevant conditions. These features enable selective covalent engagement of protein targets distinct from those typically associated with Au(I) complexes. Given the central role of mitochondrial hub proteins in regulating immunometabolic signaling, we investigated cyclometalated Au(III) bisphosphine complexes as chemical probes and identified voltage-dependent anion channel 1 (VDAC1) as a direct molecular target, providing mechanistic insight into how Au(III) complexes modulate mitochondrial function and tumor-associated immune signaling.

Advances in activity-based protein profiling (ABPP) and chemoproteomic techniques now enable systematic mapping of small molecule−protein interactions, particularly for covalent inhibitors and metallodrugs that engage unconventional binding sites.[35] In 2015, Babak et al. identified protein interactors of an antimetastatic Ru(II) compound (RAPTA) through drug affinity chromatography and subsequent LC−MS analysis of pulled down proteins.[36] Soon after, Che et al. utilized affinity-based proteome profiling to characterize the interaction between an anticancer Au(III) tetraphenyl porphyrin and heat-shock protein 60 (HSP60).[37] This was achieved by performing a click reaction between azide conjugated biotin and an alkyne probe of the gold porphyrin, followed by affinity purification with streptavidin and subsequent LC−MS/MS analysis. Recently, our lab employed a chemo-tagged biotinylation approach of an anticancer Au(III) macrocycle (Au-Mac1) to identify heme oxygenase 2 (HMOX2) as the primary target of anticancer action.[38] We posit that integration of chemical biology tools with cellular thermal shift assays (CETSA) and transcriptomics can be used to interrogate how metal center geometry and ligand architecture conspire to direct inflammatory-immune signaling—a critical step toward rational design of metallopharmaceuticals.

Here, we describe the synthesis of alkyne-functionalized AuPhos via oxime ligation to enable chemotagging through bioorthogonal click chemistry with a biotin or fluorescent tag for molecular target identification by chemical proteomics in human breast cancer, MDA-MB-231, and colon epithelial NCM-460 cell lines in a context-dependent manner. Further cellular response characterization by proteomic profiling in the two physiologically different cell lines revealed VDAC1 as a reliable target of AuPhos. Additionally, RNA-sequencing analysis showed that AuPhos-treated MDA-MB-231 cells uncovered downregulated metabolic factors, including mitochondrial respiratory electron transport chain transcripts along with a robust activation of inflammatory and immune-related transcriptional programs in tumor cells. Surprisingly, these effects were opposite in normal epithelial cells, despite the common VDAC1 target. These findings uncover a previously unrecognized mechanism by which an organogold(III) complex triggers cancer-cell-biased inflammatory reprogramming via VDAC1 engagement, establishing a framework for exploring mitochondrial immunometabolism as a targetable vulnerability in cancer.

RESULTS AND DISCUSSION

Rationale, Synthesis, and Characterization of AuPhos-Probe

To address stability limitations commonly associated with Au(III) complexes in biological environments, AuPhos incorporates a strong σ-donating chelating bisphosphine ligand framework designed to stabilize the Au(III) center while preserving controlled electrophilicity. This ligand architecture enhances kinetic and redox stability, providing a balance between physiological stability and biological reactivity.[39] Consistent with this design, AuPhos remained intact upon

https://doi.org/10.1021/jacs.6c00003
J. Am. Chem. Soc. XXXX, XXX, XXX−XXX

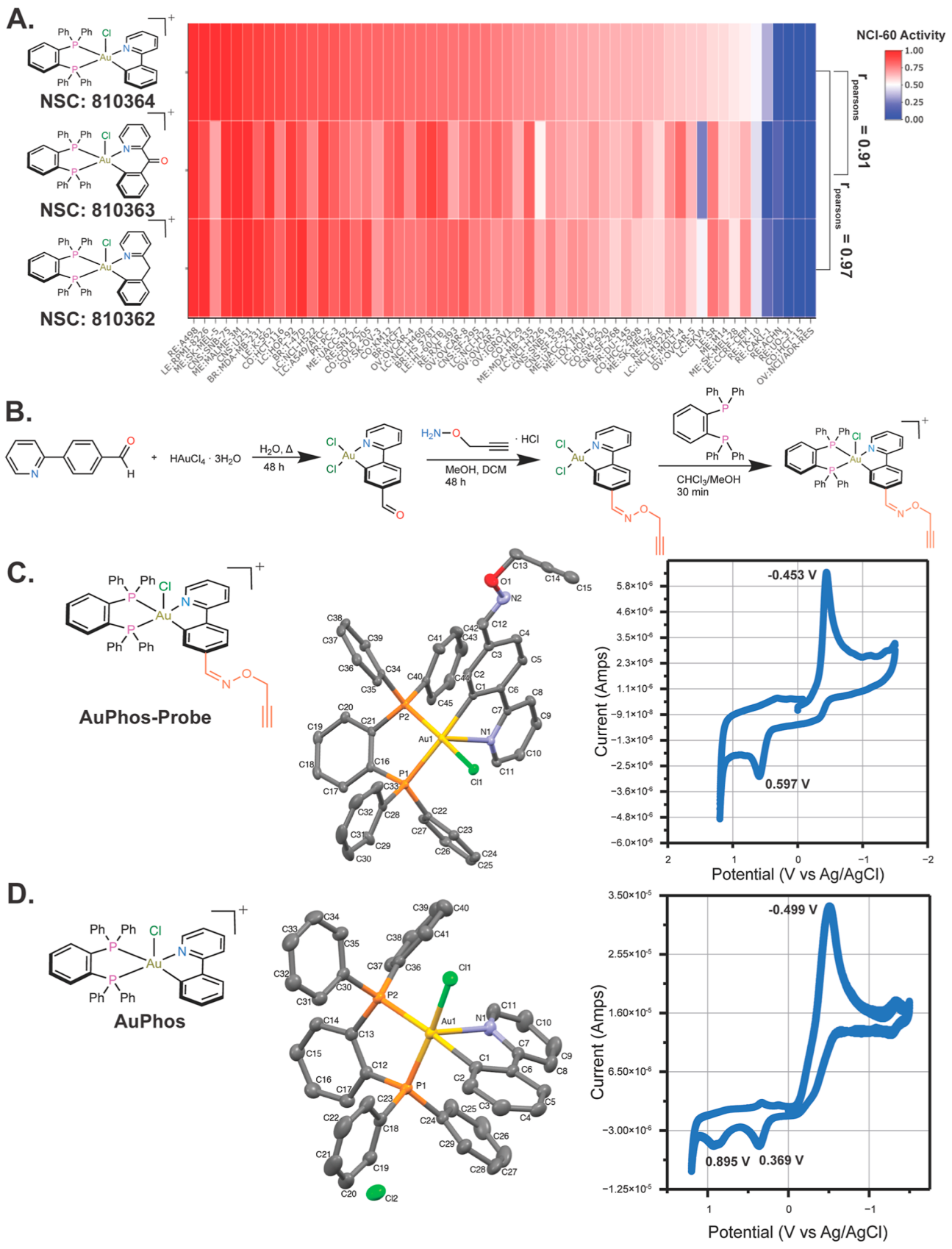

Figure 1. Phenotypic and structural characterization of AuPhos. (A) Chemical structures of AuPhos class of compounds and its corresponding heatmap of the -log10 (GI50) [concentration of agent that inhibits 50% of cell growth] values of sulforhodamine B assay in the NCI-60 screen. Pearson Correlation values are represented on the right side of the heatmap. Graphs and Pearson Correlations were generated using the CellMiner Cross Database (CBD) tool provided by the National Cancer Institute.[41] (B) Chemical synthesis of AuPhos-probe for pull-down, target identification, and chemoproteomic assays. (C) Chemical structure (left), X-ray crystal structure (center), and cyclic voltammogram (right) of AuPhos-probe. (D)

https://doi.org/10.1021/jacs.6c00003
J. Am. Chem. Soc. XXXX, XXX, XXX−XXX

Figure 1. continued

Chemical structure (left), X-ray crystal structure (center), and cyclic voltammogram (right) of AuPhos. Ellipsoids are drawn at 50%. Hydrogen atoms and counteranions of AuPhos-probe were omitted for clarity.

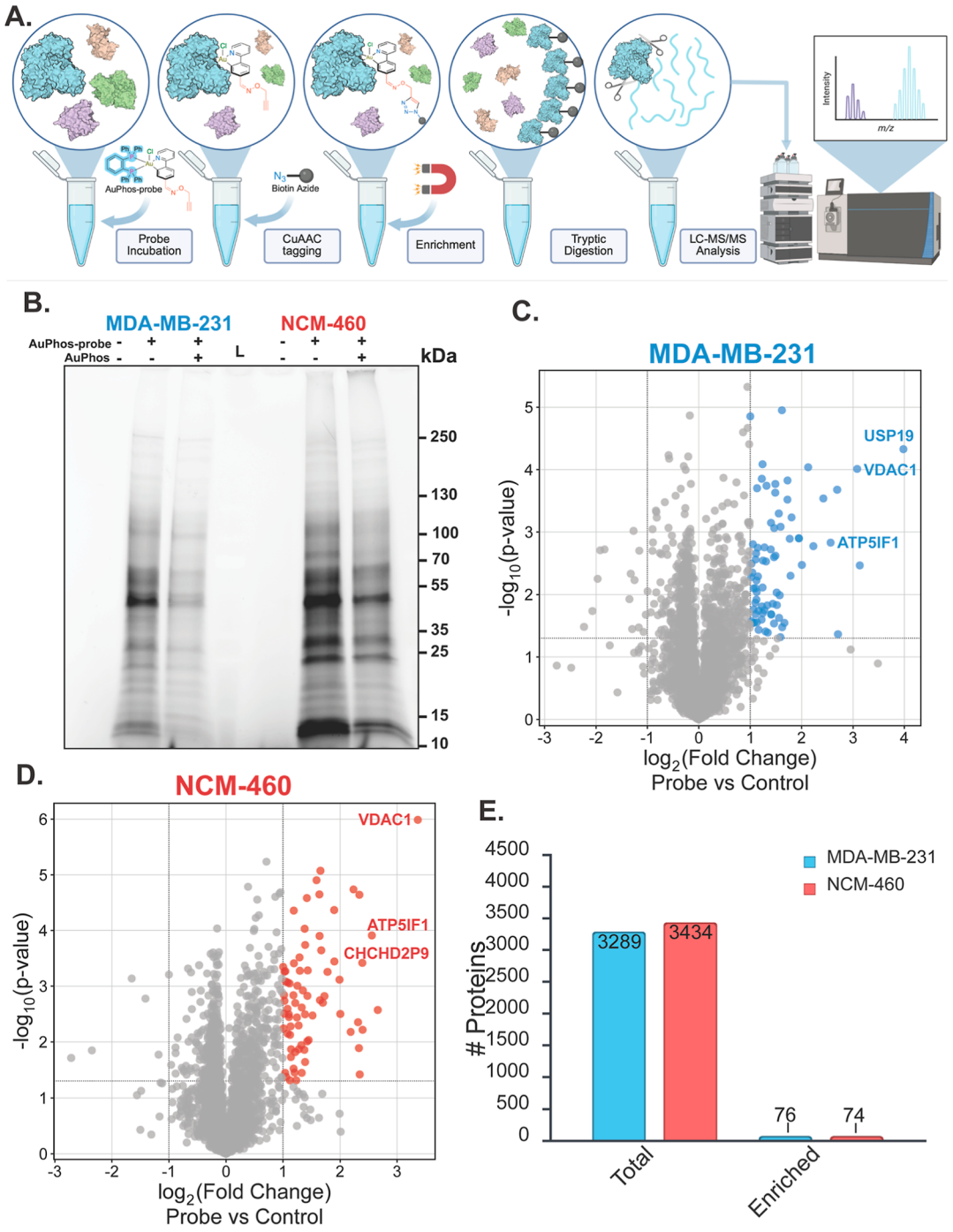

Figure 2. (A) Chemo proteomics workflow employed to identify proteins bound by AuPhos. (B) In gel fluorescence image of DMSO control or AuPhos-probe-treated lysates. (C) Volcano plots of protein enrichment and significance in MDA-MB-231 and (D) NCM-460 cell lines. (E) Bar chart of total proteins identified and enriched proteins in MDA-MB-231 (blue) and NCM-460 (red) cell lines.

incubation with excess concentrations of the cellular thiol antioxidant L-glutathione (GSH), showing no detectable decomposition over 24 h as determined by HPLC and NMR analysis, respectively (Figure S1A,B). Furthermore, treatment of nontransformed human colon epithelial cells (NCM-460) with 10 μM AuPhos followed by cell lysis and HPLC−HRMS analysis confirmed the presence of intact AuPhos, demonstrating that the complex remains stable under physiologically relevant intracellular conditions (Figure S2). Together, these findings validate the bisphosphine-stabilized Au(III) scaffold as a robust platform suitable for biological target engagement.

https://doi.org/10.1021/jacs.6c00003
J. Am. Chem. Soc. XXXX, XXX, XXX−XXX

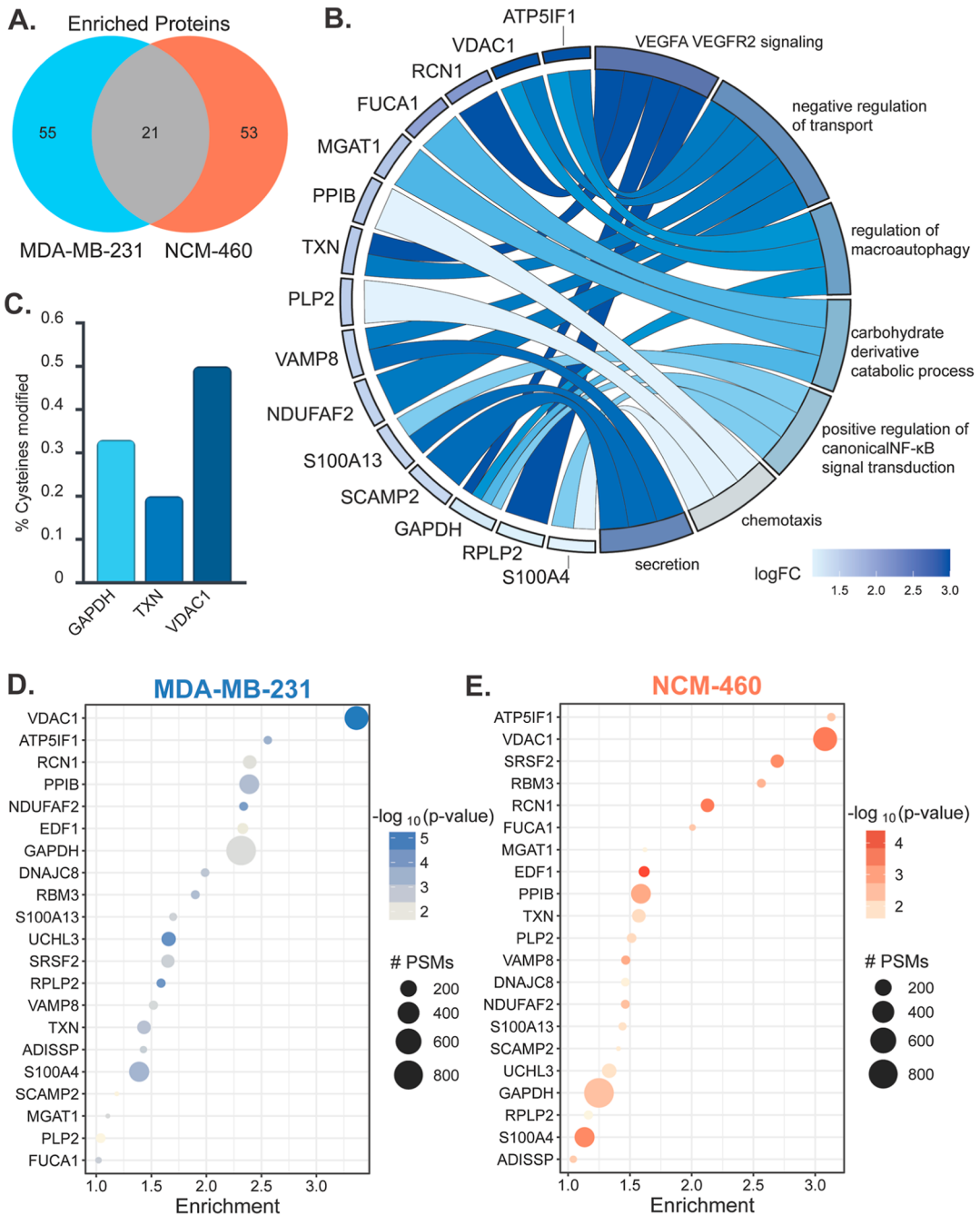

Figure 3. (A) Venn diagram of enriched proteins in MDA-MB-231 and NCM-460, identifying 21 proteins in common. (B) Circos plot of top enriched genes and enriched pathways. (C) Bar chart of the percentage of AuPhos-modified cysteines in VDAC1, TXN, and GAPDH. (D) Bubble plot of enrichment (x-axis), $-\log_{10}(p\text{-value})$ (color), and #PSMs (size) for genes found significantly enriched in both MDA-MB-231 and (E) NCM-460 cell lines.

An alkyne functionalized AuPhos − [C^N]-cyclometalated Au(III) bearing 1,2-bis(diphenylphosphino)benzene (DPPBz), where [C^N] represents 2-phenylpyridine was synthesized to enable an unbiased determination of the target landscape of AuPhos by chemical proteomics. The rationale was to use AuPhos-alkyne in an in situ Cu(I)-catalyzed azide−alkyne cycloaddition reaction with azido-biotin or azido-rhodamine in MDA-MB-231 or NCM-460 cell lysates to obtain highly efficient target enrichment while minimizing noise from biotin metabolism, off-targets, or false positives/negatives. Following analysis of the NCI-60 cancer cell line phenotypic screen of complexes in the AuPhos family, we noted that modifications of the aryl-pyridine framework of AuPhos minimally impacted GI50s indicating less pharmacophore effects and suitable for alkyne modification.[40] Using CellMinerCDB, we generated a heatmap of AuPhos and its analogs with modified aryl-pyridine ligands (Figure 1A) and the calculated Pearson's correlations showed that the activity of AuPhos and its analogs possessed strong correlations 0.91 and 0.97, respectively (Figure S3). Having established the rationale to place the terminal alkyne on the aryl-pyridine fragment of AuPhos, we employed the scheme shown in Figure 1B. First, we employed a green C−H activation protocol in water to generate cyclometalated 4-(2-pyridyl)-benzaldehyde Au(III)Cl_2. Condensation of the aldehyde

https://doi.org/10.1021/jacs.6c00003
J. Am. Chem. Soc. XXXX, XXX, XXX−XXX

functional group with O-2-propynylhydroxylamine hydrochloride afforded a [C^N]-cyclometalated Au(III) complex bearing an aldoxime-linked terminal alkyne. Chelation with DPPBz in a mixture of chloroform and methanol resulted in the AuPhos-alkyne probe to be used in pull-down, target identification, and chemoproteomic assays. Characterization and purity of the complexes were ascertained by ^{1}H, ^{13}C, and $^{31}P[^{1}H]$ nuclear magnetic resonance (NMR) spectroscopy, and high-performance liquid chromatography electrospray ionization mass spectrometry (HPLC-ESI-MS, Figures S4−S14). Structural elucidation of the complexes was obtained via single crystal X-ray diffraction analysis, showing a distorted square pyramidal geometry with a fifth coordination elongated chlorine bond to the Au^{III} center (Figure 1C,D and Table S2). Electrochemical behavior of both AuPhos and AuPhos-probe was then assessed by cyclic voltammetry, which showed a signature reduction event of −0.499 V (Figure 1C, right) and −0.453 V (Figure 1D, right), respectively, demonstrating electrochemical stability for a Au^{III}/Au^{I} couple.

Chemoproteomic Profiling of AuPhos

On the basis of our phenotypic screening across the NCI-60 cancer cell line panel, triple-negative breast cancer (TNBC) cell lines, along with several other tumor types, exhibited marked sensitivity to AuPhos. Among these, the MD Anderson-Metastatic Breast-231 (MDA-MB-231) cell line was selected as the primary model for this study due to its well-established representation of aggressive, basal-like TNBC and its metabolic and proteomic features that reflect the functional heterogeneity characteristic of this disease subtype. These properties make MDA-MB-231 cells particularly suitable for investigating mechanisms involving the mitochondrial and proteostasis pathways. Notably, VDAC1 is highly expressed and functionally important in TNBC, further supporting the relevance of this model for studying the AuPhos mechanism of action. To complement these studies and enable identification of physiologically relevant protein interactors, the immortalized nonmalignant human colonic epithelial cell line NCM-460 was used as a nontransformed comparator. This model provided a biologically relevant normal cellular context for chemical proteomic analysis and target identification.[42]

To identify the protein interactors of AuPhos, we performed an in vitro CuAAC click chemistry reaction of the synthesized AuPhos-probe and azido-biotin or azido rhodamine in MDA-MB-231 and NCM-460 cell lysates. The workflow employed is shown in Figure 2A. First, protein labeling was achieved through incubation of AuPhos-probe in freshly prepared cell lysates. Following this, probed proteins were tagged with azido-biotin through CuAAC click chemistry. Incubation with magnetic streptavidin beads allowed for the purification of probe-tagged proteins due to the strong and selective interaction between biotin and streptavidin. Subsequent peptide digestion and liquid chromatography-tandem mass spectrometry (LC−MS/MS) were employed to identify peptides and proteins pulled down by the AuPhos probe.

To verify the efficacy of AuPhos-probe toward labeling proteins and subsequent azide-mediated tagging, we performed in-gel fluorescence with rhodamine-azide. As shown in Figure 2B, fluorescent bands are observed in MDA-MB-231 and NCM-460 in a manner dependent on the presence of the AuPhos probe. In separate lysates, we incubated AuPhos before the addition of AuPhos-probe and visually assessed changes in fluorescent protein bands. We observed decreased intensities for all protein bands upon AuPhos competition. Decreased band intensities are most likely due to saturation of binding sites by AuPhos that prevents AuPhos-probe labeling. This indicates that AuPhos and AuPhos-probe have similar binding profiles.

We then performed chemoproteomic profiling and identified enriched proteins through LC−MS/MS analysis. Using proteins present in all samples per cell line, we identified peptides for 3289 proteins in MDA-MB-231 and 3434 proteins in NCM-460 cell lysates. The sum of peak intensities of each peptide for each protein was calculated as the abundance of the protein pulled down. Assuming each sample contains similar amounts of total protein, sum normalization of protein abundances was performed to allow robust comparative analysis between treatment conditions. To determine the probability that a protein's abundance changed due to the presence of AuPhos-probe, an independent *t*-test was performed on the abundances between PBS-treated controls and AuPhos-probe-treated samples. In concert, enrichment upon AuPhos-probe treatment was calculated as the $\log_2$(fold change) of a protein's abundance in the probe-treated group divided by its abundance in the control group. Volcano plots of enrichment and −log10 *p*-value are shown in Figure 2C,D. Out of the 3289 proteins identified in MDA-MB-231, 76 proteins had a $\log_2$-fold change >1, *p*-value <0.05, and were considered as enriched (Figure 2E). Using the same enrichment criteria, we found 74 enriched proteins in NCM-460, out of the 3434 identified. We found the top significantly enriched proteins in MDA-MB-231 lysates are USP19, VDAC1, and ATP5IF1, while in NCM-460 cell lysates, VDAC1, CHCHD2P9, and ATP5IF1 were the top significantly enriched proteins.

Identification of VDAC1 as the Top Target of AuPhos

To identify the top target of AuPhos, we closely examined enriched proteins in MDA-MB-231 and NCM-460 to identify those enriched in both cell lines. We found 21 proteins that were enriched in both cell lines and prioritized those as the highly ranked targets of AuPhos (Figure 3A). Gene annotation and analysis revealed that the top targets relate to pathways of VEGFA/VEGFR2 signaling, negative regulation of transport, macroautophagy, carbohydrate derivative catabolism, NF-κB signal transduction, chemotaxis, and secretion consistent with VDAC modulation (Figure 3B). Importantly, we performed deep analyses of our proteomics data set for potential cysteine modification given that AuPhos is a [C^N]-cyclometalated Au^{III} tuned for targeted cysteine arylation within the proteome. We found that three of the top 21 protein targets contained peptide modifications—VDAC1, GAPDH, and TXN. Out of these three, VDAC1 had the highest percentage of available cysteines modified by AuPhos (Figure 3C). To further distinguish the top protein target from the 21 enriched proteins, we examined the number of peptide spectrum matches (PSMs) for each protein. Peptide spectrum matches are the number of observed mass spectra assigned to a peptide sequence contributing to a protein's abundance and indicate the relative abundance of a protein in the sample. Bubble plots of the enrichment, $-\log_{10}$(*p*-value), and number of PSMs for each protein are shown in Figure 3D,E. In addition, in ensuring unbiased identification of bona fide AuPhos targets, we applied multiple orthogonal criteria, including reproducible enrichment across biological systems, evidence of probe-dependent covalent modification, and peptide identification confidence (Table S3). First, candidate proteins were required to show reproducible enrichment in both MDA-MB-231 and NCM-460 cells. While

https://doi.org/10.1021/jacs.6c00003
J. Am. Chem. Soc. XXXX, XXX, XXX−XXX

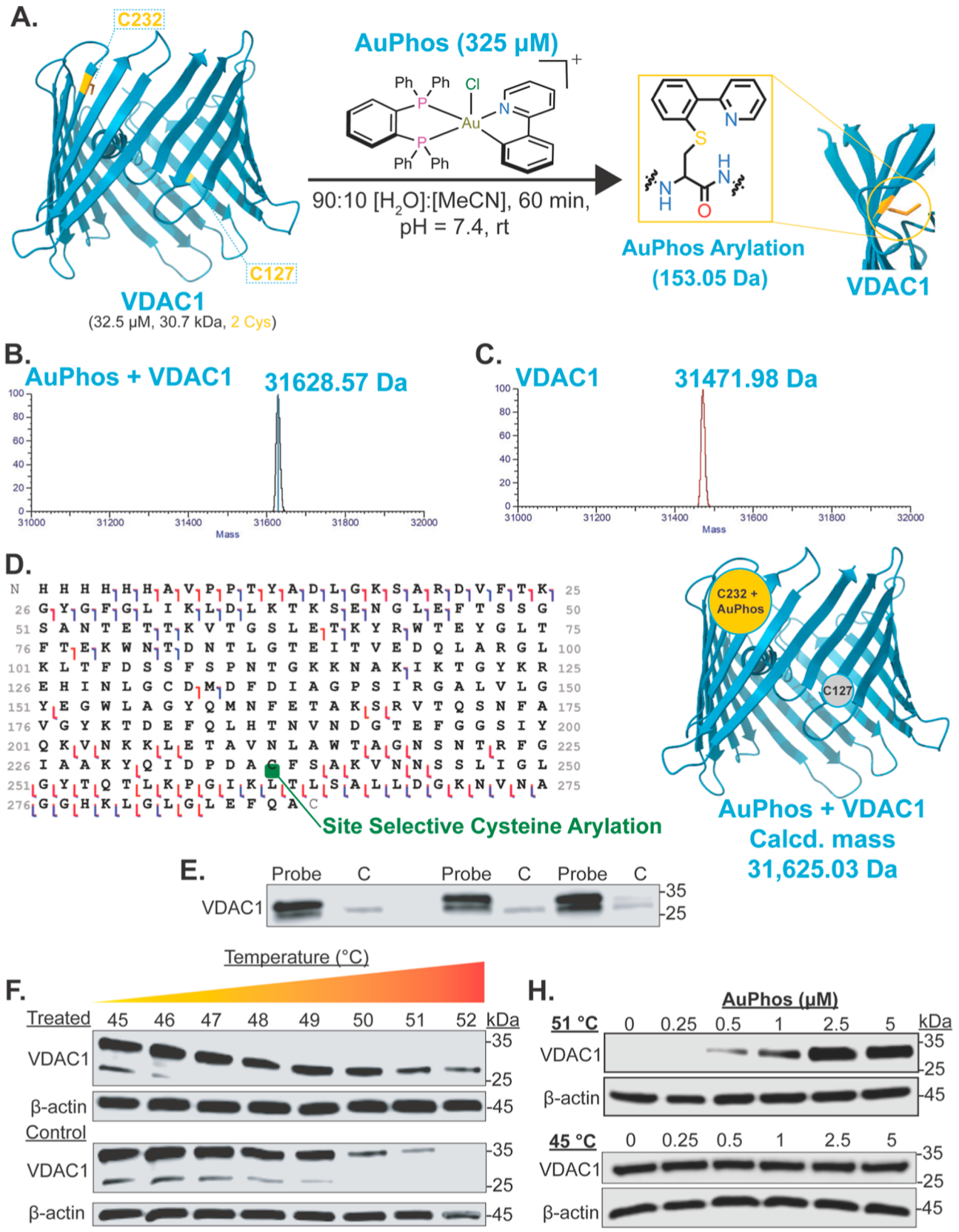

Figure 4. (A) Schematic of reaction employed in the intact mass analysis of AuPhos incubated with VDAC1. (B) Mass spectra of AuPhos incubated with VDAC1. (C) Mass spectra of VDAC1 in the conditions used in the intact mass experiment. (D) Peptide map and VDAC1 protein image from top-down proteomics identifying selective modification of C232 by AuPhos. (E) Western blot of streptavidin beads from the protein pulldown experiments with PBS control or probe-treated lysates. (F) Western blot examining the level of solubilized VDAC protein in MDA-MB-231 cell lysates at increasing temperatures. Live cells were treated with AuPhos (top images) or a DMSO control (bottom). (H) Isothermal dose–response CETSA (ITDR-CETSA) in MDA-MB-231 cells demonstrating dose-dependent thermal stabilization of VDAC1 beginning at 0.5 μM AuPhos.

https://doi.org/10.1021/jacs.6c00003
J. Am. Chem. Soc. XXXX, XXX, XXX−XXX

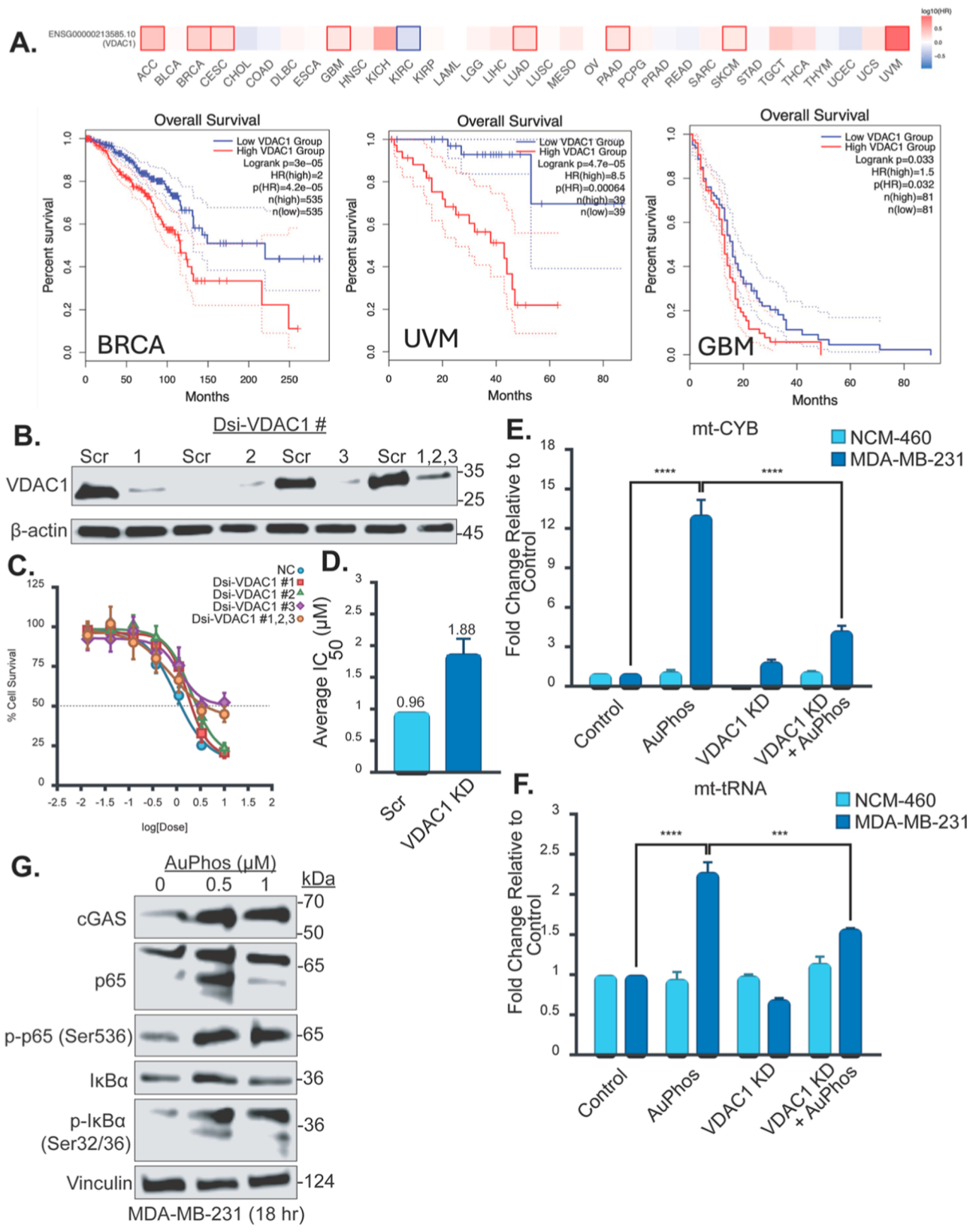

Figure 5. (A) Expression analysis of VDAC1 and overall survival in human tumors establishes VDAC1 as viable therapeutic target in cancer. (B) Western blot of VDAC1 protein levels of MDA-MB-231 following transfection of scrambled Dsi-RNA or Dsi-VDAC1. (C) Cell survival curves of Dsi-RNA transfected cells following AuPhos treatment. (D) Bar chart of the average IC_{50} of scrambled versus Dsi-VDAC1 transfected cells following AuPhos treatment. (E) Bar chart representing the relative fold change of mt-CYB dsDNA in the cytoplasm of NCM-460 and MDA-MB-231 cell lines after 18 h of AuPhos treatment. (F) Bar chart representing the relative fold change of mt-tRNA dsDNA in the cytoplasm of NCM-460 and MDA-MB-231 cell lines after 18 h of AuPhos treatment. (G) Western blot examining protein levels of cGAS, NF-κB, p−NF−κB, IκB-α, and *p*-IκB-α in MDA-MB-231 cells after 18 h treatment of AuPhos at varying concentrations.

https://doi.org/10.1021/jacs.6c00003
J. Am. Chem. Soc. XXXX, XXX, XXX−XXX

USP19 showed enrichment in MDA-MB-231 cells, it was not significantly enriched in NCM-460 cells, suggesting cell-type-specific enrichment and reducing confidence in it as a primary and generalizable molecular target of AuPhos. Second, we evaluated direct evidence of covalent probe engagement through identification of AuPhos-modified peptides. ATP5IF1 did not contain detectable AuPhos-modified peptides and was supported by relatively low peptide spectral matches (PSMs), indicating lower confidence in direct probe engagement. In contrast, VDAC1 satisfied all selection criteria, including robust enrichment across both cell lines, clear identification of AuPhos-modified peptides, and high PSM counts. Additionally, VDAC1 is a mitochondrial outer membrane protein with established roles in metabolic regulation, consistent with the observed mitochondrial and immunometabolic phenotypes. Together, these factors provided strong evidence supporting VDAC1 as a direct and biologically relevant molecular target of AuPhos.

AuPhos Stabilization of VDAC1 In Vitro

To validate the observed enrichment of VDAC1 from our robust chemoproteomic profiling, we performed intact mass analysis followed by top-down proteomics of VDAC1 incubated with AuPhos and performed additional pull-down studies using the described CuAAC reaction in lysates of MDA-MB-231 cells followed by SDS-PAGE and Western blotting to analyze for VDAC1. Intact mass analysis was performed by incubating AuPhos with VDAC1 at a 10:1 ratio in a solution of water and acetonitrile for 1 h at room temperature (Figure 4A). Similar to other Au^{III} arylation reagents,[34] we found a 156.59 Da difference in the mass of VDAC1 when incubated with AuPhos correlating to the aryl-pyridine ligand (Figure 4B,C). We then pursued top-down proteomics and found that cysteine 232 was selectively modified by AuPhos (Figure 4D). We then used streptavidin-coated beads from AuPhos-probe-treated lysates and found strong band intensities upon immunoblotting for VDAC1, confirming the enrichment of VDAC1 dependent on AuPhos-probe (Figure 4E). Subsequently, we investigated cellular target engagement of AuPhos in live cells by cellular thermal shift assay (CETSA), an assay designed to examine the effect of drug binding on the thermal stability of a protein. To do this, healthy MDA-MB-231 cells were treated with AuPhos or vehicle control at a concentration of 10 μM for 2 h. Cells were then subjected to heat treatment at a range of 45 °C to 52 °C. The amount of solubilized VDAC protein at each temperature was assessed by SDS-PAGE and immunoblotting. In cells treated with AuPhos, we found a greater level of solubilized VDAC upon temperature increase compared to DMSO-treated cells (Figure 4F). This is demonstrated in melting curves of three biological replicates where a ~0.9 °C thermal stabilization of VDAC1 is observed after AuPhos treatment (Figures S17 and S18). We then performed isothermal dose−response CETSA (ITDR-CETSA) and determined that AuPhos-induced VDAC1 stabilization begins at a concentration of 0.5 μM (Figure 4H). Taken together, the novel engagement of VDAC1 by AuPhos is demonstrated.

VDAC1 Is a Viable Cancer Target

Targeting hub proteins represents a transformative strategy to overcome key cancer hallmarks, including metabolic reprogramming, therapy resistance, and uncontrolled cell proliferation. Among these, VDAC1 stands out as a mitochondrial gatekeeper with emerging therapeutic potential. VDAC1 is in the outer mitochondrial membrane (OMM), where it facilitates the transfer of critical metabolites, ions (including Ca^{2+}), fatty acids, cholesterol, and reactive oxygen species (ROS) across the OMM, thus playing a central role in cellular metabolism and mitochondrial-mediated apoptosis. The VDAC protein family consists of three isoforms, VDAC1, VDAC2, and VDAC3, with VDAC1 being the most abundant and functionally dominant. In aggressive and therapy-resistant tumors, VDAC1 is frequently overexpressed, correlating with tumor aggressiveness, resistance to therapy, and poor clinical outcomes (Figure 5A, data from TCGA). We performed Western blot on a panel of cancer cell lines and normal MCF10A and validated the increased expression of VDAC1 (Figure S19). This makes VDAC1 not only a biomarker of cancer progression but also a promising therapeutic target. We are actively developing novel VDAC1 modulators aimed at treating metabolically vulnerable tumors, including Hürthle cell carcinoma, melanoma, central nervous system (CNS) tumors, renal cancer, prostate cancer, and triple-negative breast cancer (TNBC). To confirm that AuPhos is selectively targeting VDAC1 in vitro, we used RNA interference (RNAi) to knock-down VDAC1 in MDA-MB-231 cells. We transfected MDA-MB-231 cells with Dsi-RNA targeting VDAC1 at an efficiency of 97.0% (Figure S20). After incubation for 96 h, we found substantial knockdown of VDAC1 (Figures 5B and S21). We then performed cell viability studies of AuPhos-treated scrambled and VDAC1-KD cells and plotted cell survival curves (Figure 5C). We found that the average IC_{50} of AuPhos-treated VDAC1-KD cells was 1.88 μM, a significant reduction from the IC_{50} of scrambled cells (0.96 μM, Figure 5D). This result demonstrates that VDAC1 engagement fuels the cytotoxicity of AuPhos in cancer cell lines. We posit that the AuPhos-VDAC1 interaction may release mitochondrial DNA to the cytosol to drive immunometabolic reprogramming resulting in cancer cell death. To test this, we isolated cytoplasmic fractions of NCM-460 and MDA-MB-231 cells and ran RT-qPCR for mt-CYB and mt-tRNA dsDNA (Figure 5E,F). After normalizing to cytoplasmic protein, we found that AuPhos treatment significantly elevated cytoplasmic mt-CYB and mt-tRNA genes in cancerous MDA-MB-231 and not NCM-460. When VDAC1 was knocked-down, this effect was significantly diminished, indicating that upregulation of mt-DNA in the cytoplasm confirming that the VDAC1-AuPhos interaction is the primary driver of this linkage. We then performed Western blot to examine if the increased cytoplasmic mt-DNA results in activation of the cGAS-STING−NF−κB axis. We found that levels of cyclic GMP-AMP synthase increase after 18 h treatment of AuPhos in MDA-MB-231 cells (Figures 5G, S22, and S23), consistent with increased mtDNA in the cytosol. Additionally, protein levels of NF-κB (p65) and phosphorylated NF-κB (p-p65) are increased at concentrations of 0.5 μM compared to control. We also observed increased phosphorylated nuclear factor of κB inhibitor α (p-IκB-α), and increased p-IκB-α/total p-IκB-α ratio, both indicators of the phosphorylation and degradation of IκB-α, which is a key step toward increasing protein levels of NF-κB (Figure S23). This further supports NF-κB activation. Taken together, these results indicate that the mt-DNA released to the cytoplasm prevents NF-κB degradation and promotes its activation. Together, these data provide a comprehensive molecular mechanism in which AuPhos targets VDAC1 to induce cytosolic mtDNA release, which subsequently activates the cGAS-mediated inflammatory response. Additionally, coimmunoprecipitation studies to identify interactive effects of VDAC1 binding partners such as β-tubulin and HK2 confirmed enrichment of VDAC1-β-tubulin in the presence of AuPhos. We found that AuPhos may be disrupting

https://doi.org/10.1021/jacs.6c00003
J. Am. Chem. Soc. XXXX, XXX, XXX−XXX

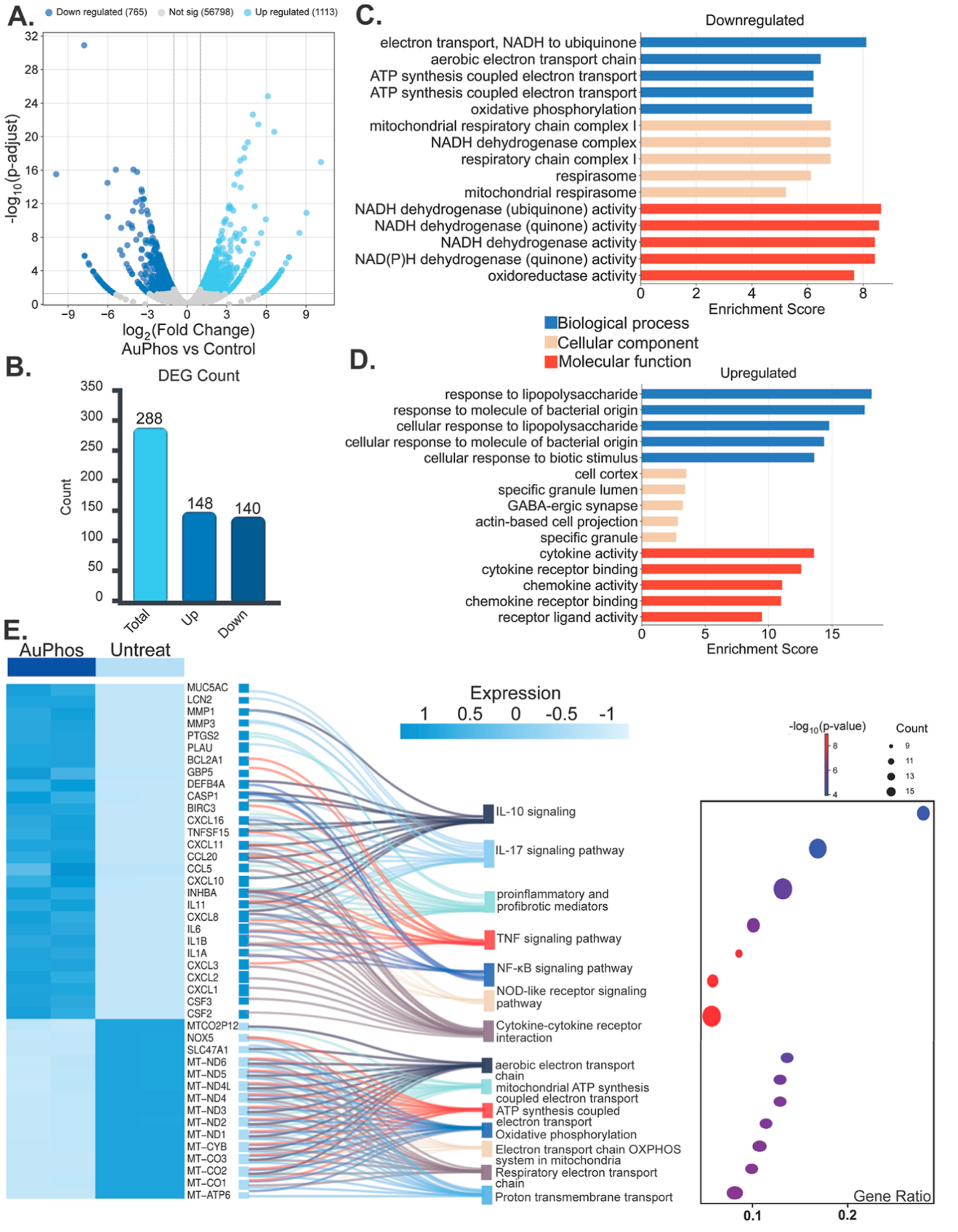

Figure 6. (A) Volcano plot of DESeq2 calculated $\log_2$(fold change) and -$\log_{10}$(p-adjust) for transcript expression level changes in AuPhos vs control-treated cells. (B) Bar chart of the count of total, upregulated, and downregulated transcripts. (C) Bar charts of enriched Gene Ontology terms for upregulated transcripts and (D) downregulated transcripts upon AuPhos treatment. (E) Heatmap of transcripts differentially expressed upon AuPhos treatment. Genes are connected to a bubble chart of enriched pathways with a Sankey plot.

https://doi.org/10.1021/jacs.6c00003
J. Am. Chem. Soc. XXXX, XXX, XXX−XXX

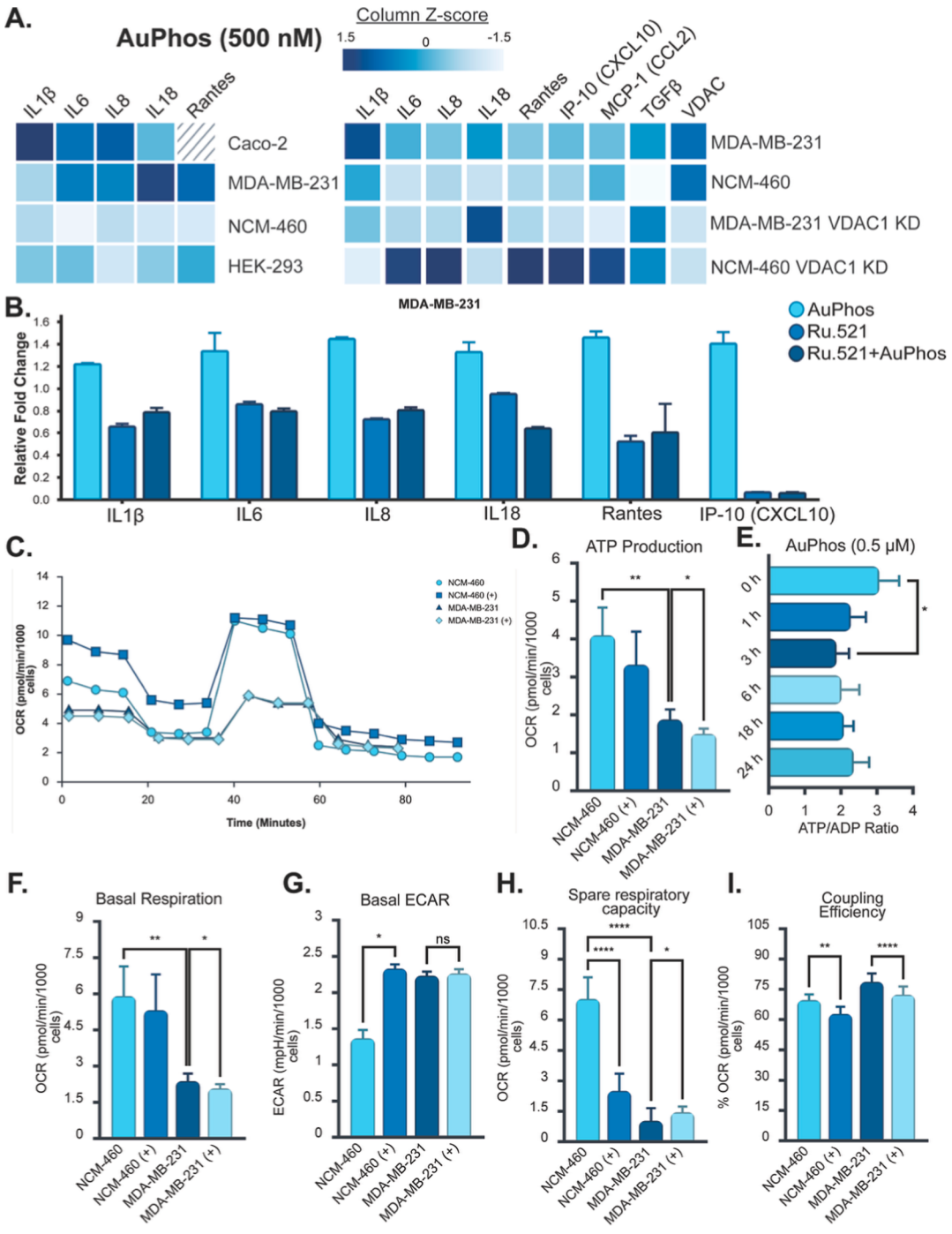

Figure 7. (A) Heatmap of key NF-κB cytokine mRNAs in MDA-MB-231, NCM-460, Caco-2, and HEK-293 cell lines (left). Heatmap of key NF-κB cytokine mRNAs in MDA-MB-231, NCM-460 with or without VDAC1 KD via siRNA transfection (right). (B) Relative fold change (to control) of key NF-κB cytokine mRNAs in MDA-MB-231 with 1 h Ru.521 (10 μM) pretreatment, and/or AuPhos (0.5 μM). (C) OCR graph of NCM-460 and MDA-MB-231 cell lines treated with or without 500 nM AuPhos, assessed by the Seahorse XF mitostress test. (D) ATP linked respiration measurements of AuPhos (+)-treated NCM-460 and MDA-MB-231 cells. (E) ATP/ADP ratio luminescence assay of MDA-MB-231 cells treated with AuPhos (0.5 μM) at varying time points. (F) Basal respiration measurements of AuPhos (+)-treated NCM-460 and MDA-MB-231 cells. (G) Basal ECAR measurements of AuPhos (+)-treated NCM-460 and MDA-MB-231 cells. (H) Spare respiratory measurements of AuPhos (+)-treated NCM-460 and MDA-MB-231 cells. (I) Coupling efficiency measurements of AuPhos (+)-treated NCM-460 and MDA-MB-231 cells.

VDAC1-HK2 interaction due to decreased HK2 enrichment from the co-IP study. This may be influencing cytotoxicity and signaling outcomes observed (Figure S25).

AuPhos Stimulates Cancer Specific Immune Signaling Pathways

Mitochondria play a central role in cancer progression through their regulation of cellular metabolism and signaling.[43] Among mitochondrial proteins, VDAC1 is highly abundant on the outer membrane and functions as a critical gatekeeper of mitochon-

https://doi.org/10.1021/jacs.6c00003
J. Am. Chem. Soc. XXXX, XXX, XXX−XXX

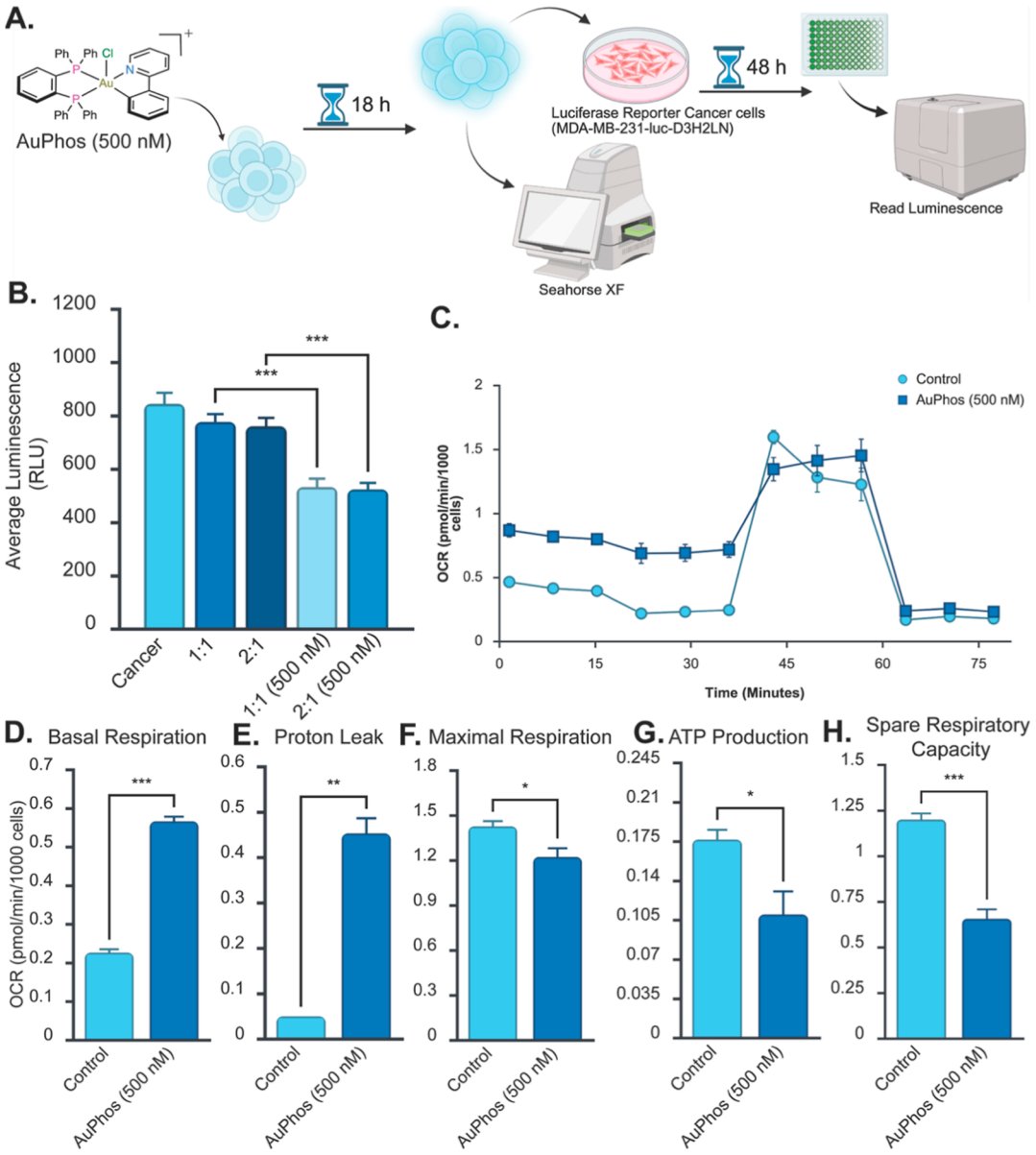

Figure 8. (A) Schematic of experiments performed to assess effects of AuPhos stimulation on respiration of PBMCs and cancer cell killing abilities. (B) Bar charts of the average luminescence of cancer cells cocultured at ratios of unstimulated versus AuPhos (500 nM)-stimulated PBMCs. (C) OCR graph of PBMCs stimulated with AuPhos at 500 nM. (D) Basal respiration measurements of AuPhos-treated PBMCs. (E) Proton leak measurements of AuPhos-treated PBMCs. (F) Maximal respiration measurements of AuPhos-treated PBMCs. (G) ATP production measurements of AuPhos-treated PBMCs. (H) Spare respiratory measurements of AuPhos-treated PBMCs.

drial homeostasis, influencing numerous cellular processes.[44] To investigate the transcriptional consequences of AuPhos-VDAC1 interaction, we performed bulk RNA sequencing (RNA-seq) in MDA-MB-231 cells. Differential expression analysis revealed 148 transcripts upregulated and 140 downregulated upon AuPhos treatment (Figure 6A,B). Overrepresentation analysis of these differentially expressed genes highlighted distinct functional signatures. Downregulated transcripts were predominantly enriched in gene ontology (GO) terms and pathways associated with mitochondrial electron transport (Figure 6C,E), consistent with AuPhos-induced mitochondrial membrane depolarization in MDA-MB-231 cells.[27] Conversely, upregulated transcripts were significantly associated with immune and inflammatory responses, including GO terms such as response to lipopolysaccharide, cytokine activity, and chemokine activity (Figure 6D). Corresponding enriched pathways encompassed IL-10, IL-17, TNF, NF-κB, and NOD-like receptor signaling (Figure 6E). Increase of these pathways is expected given that AuPhos-VDAC1 interaction increased cytoplasmic mtDNA in MDA-MB-231 cells. Specifically, IL-10 transcription is activated by NF-κB as a cellular response mechanism to inflammatory stress. These findings suggest that AuPhos activates cancer-specific immune signaling pathways, potentially through VDAC engagement, which has been implicated in NLRP3 inflammasome activation[45] and interferon signaling.[15]

AuPhos Induction of Cytokine Transcription and Mitochondrial Modulation

It is known that VDAC has altered regulation in cancerous cells compared to normal, exemplified by studies demonstrating free tubulin binds VDAC and inhibits formation of mitochondrial membrane potential in cancer cells but not in primary rat

https://doi.org/10.1021/jacs.6c00003
J. Am. Chem. Soc. XXXX, XXX, XXX−XXX

hepatocytes.[46] Given this, we sought to examine the effects of the AuPhos-VDAC1 interaction on cancerous cell lines MDA-MB-231 (breast) and Caco-2 (colorectal) compared to the normal epithelial cell lines NCM-460 (colon) and HEK-293 (kidney). To do this, we treated the cell lines with AuPhos (500 nM) overnight and compared the mRNA levels of key cytokines/chemokines in the NF-κB pathway with RT-qPCR (Figure 7A, left). We observed greater expression of IL-6, IL-8, and IL-18 mRNAs in the cancerous cell lines compared to normal. When comparing the cancerous Caco-2 to normal NCM-460, we see increased expression of IL-1β. To validate that this effect is dependent on an AuPhos-VDAC1 interaction, we performed the same experiment after generating MDA-MB-231 and NCM-460 VDAC1 knock-down cells (Figure 7A, right). In MDA-MB-231, knockdown of VDAC1 significantly attenuated the AuPhos-induced upregulation of IL-1β, IL-6, IL-8, IP-10, and MCP-1. In NCM-460, knockdown of VDAC1 resulted in the elevation of IL-6, IL-8, RANTES, IP-10, MCP-1, and TGFβ mRNAs. This result confirms that the AuPhos-VDAC interaction activates NF-κB cytokines in MDA-MB-231 cells and suppresses it in NCM-460. Given that AuPhos treatment increased cytoplasmic mt-DNA, we tested if transcriptional upregulation observed in MDA-MB-231 can be attributed to cGAS signaling. To do this, we pretreated cells with 10 μM Ru.521, a potent cGAS inhibitor, before treatment with 0.5 μM AuPhos (Figure 7B).[47] We found that Ru.521 pretreatment ablated AuPhos's ability to increase mRNA transcripts of key inflammatory cytokines/chemokines. We posit that this drastic difference may be attributed to inherent immunometabolic programming differences in carcinomas. This is exemplified by analysis of the oxygen consumption rate (OCR) of NCM-460 versus MDA-MB-231 cell lines (Figure 7C). MDA-MB-231 cells demonstrate a lower level of ATP linked respiration than NCM-460 (Figure 7D), and upon AuPhos treatment overnight this level is significantly reduced. This is consistent with mitochondrial membrane potential depolarization observed when MDA-MB-231 cells are treated with AuPhos (Figure S22). We then examined the ATP/ADP ratio of MDA-MB-231 via a luminescent reaction and found a significant reduction of the ATP/ADP ratio 3 h after AuPhos treatment, likely due to the decrease in ATP linked respiration induced by AuPhos (Figure 7E). Further, basal respiration of MDA-MB-231 is significantly lower than NCM-460 and is reduced further via AuPhos treatment (Figure 7F). The extracellular acidification rate (ECAR) of MDA-MB-231 cells did not change upon treatment with AuPhos, suggesting that the lack of ATP in cancer does not result in increased glycolysis (Figure 7G) and may be attributed to the Warburg phenotype of cancer cells. On the other hand, treatment of AuPhos increases the ECAR of NCM-460 cells, suggesting the AuPhos-VDAC1 interaction stimulated glycolysis in normal cell lines. Lastly, we find that AuPhos significantly decreases spare respiratory capacity in NCM-460 while elevating it in MDA-MB-231 and decreasing coupling efficiency in both cell lines (Figure 7H,I). Taken together, AuPhos confers cell-line dependent immunometabolic reprogramming in breast cancer vs epithelial model systems.

AuPhos Enhances T-Cell-Mediated Killing of Cancer Cells

Inspired by increased transcription of cytokines and chemokines observed by RNA sequencing and RT-qPCR, we hypothesized that AuPhos may enhance the ability of T-cells to kill cancer cells. Therefore, we stimulated IL-2 cultured human peripheral blood monocytes (PBMCs) with AuPhos for 18 h and examined their respiratory activity and ability to kill cancer cells (Figure 8A). To isolate the effect of AuPhos on the immune cells, we utilized a prestimulation and "washout" protocols. Isolated PBMCs were incubated with media containing AuPhos for 18 h. Following stimulation, the PBMCs were centrifuged and resuspended in fresh, compound-free media to ensure the complete removal of any residual AuPhos. These "primed" PBMCs were then introduced to the cancer cell cultures. We employed MDA-MB-231-luc-D3H2LN cells that stably express firefly luciferase and measured their luminescence following addition of luciferin to ensure robust viability measurement of cancer cells following coculture with stimulated PBMCs. We found that AuPhos significantly enhanced T-cell killing of cancer cells at both 1:1 and 2:1 ratios of PBMCs/reporter cells (Figure 8B). Respiratory analysis showed increased basal respiration of PBMCs following AuPhos treatment (Figure 8C,D). Additionally, we observed increased proton leak, decreased maximal respiration, decreased ATP production, and decreased spare respiratory capacity (Figure 8E–H). In all, AuPhos has the ability to stimulate basal levels of mitochondrial respiration in PBMCs to enhance their ability to kill cancer cells. We demonstrate that AuPhos induces immune-enhancing effects in coculture systems. However, limitations associated with genetic manipulation of PBMCs, particularly the risk of introducing confounding immunogenic effects—precluded VDAC1 knockdown studies in these cells to directly assess its role. Elucidating this mechanism in PBMCs will be the focus of future investigations, as it falls beyond the scope of the present study.

CONCLUSION

In recent years, gold (Au)-containing compounds have emerged as promising therapeutic agents toward the treatment of disease.[17] This is in part due to their ability to modulate inflammatory/immune signaling pathways, including TLR4,[21] NF-κB,[22,28] TGFβ1,[29] and the cancer antioxidant network.[24,30] Despite well-documented mechanisms, the direct molecular target for the majority of Au compounds remains unknown—a critical step toward rational design of metallopharmaceuticals. We address this challenge by investigating the direct molecular target of a series of cyclometalated Au(III) complexes bearing bisphosphine ligands (AuPhos). In cancer, AuPhos can localize to mitochondria, alter mitochondrial respiration, and inhibit tumor growth in vitro and in vivo.[27] To identify the molecular target, we synthesized an alkyne-functionalized AuPhos via oxime ligation. This enabled us to perform chemo-tagging through bioorthogonal click chemistry with a biotin or fluorescent tag for molecular target identification by chemical proteomics in human breast cancer, MDA-MB-231 and colon epithelial NCM-460 cell lines in a context-dependent manner. Further cellular response characterization by proteomic profiling in the two physiologically different cell lines revealed the voltage-dependent anion channel 1 (VDAC1) as a reliable target of AuPhos. In vivo incubation with AuPhos increased the thermal stability of VDAC1, confirming that AuPhos interacts with VDAC in live cells.

The tumor microenvironment is shaped not only by intrinsic oncogenic signaling but also by metabolic and immunological cues that dictate therapeutic responses. Exploiting metabolic stress pathways to trigger context-dependent cytokine induction within cancer cells offers a promising approach to rewire immune signaling. Due to VDAC1's role as a key gatekeeper of

https://doi.org/10.1021/jacs.6c00003
J. Am. Chem. Soc. XXXX, XXX, XXX−XXX

mitochondrial function and implications in numerous cellular processes,[44] we investigated the transcriptional response evoked by the AuPhos-VDAC interaction in MDA-MB-231 cancer cells. This uncovered downregulated metabolic factors, including mitochondrial respiratory electron transport chain transcripts, along with a robust activation of inflammatory and immune-related transcriptional programs in tumor cells. This result links VDAC1 engagement to immunometabolic reprogramming and tumor cell inflammation. Surprisingly, these effects were opposite in normal epithelial cells despite the common VDAC1 target. While intact and top-down mass spectrometry identified Cys232 as the site of covalent modification, further studies are required to determine the extent to which this specific residue contributes to the downstream cellular phenotypes observed. Future investigations employing site-directed mutagenesis will help define the mechanistic contribution of this modification to AuPhos-mediated cellular responses. These findings uncover a previously unrecognized mechanism by which an organogold(III) complex triggers cancer cell–biased inflammatory reprogramming in breast cancer versus nonmalignant model systems via VDAC1 engagement, establishing a framework for exploring mitochondrial immunometabolism as a targetable vulnerability in cancer.

■ ASSOCIATED CONTENT

Supporting Information

The Supporting Information is available free of charge at https://pubs.acs.org/doi/10.1021/jacs.6c00003.

RNA-sequencing data (XLSX)

Normalized Proteomics - Data for Figures 2 & 3 (XLSX)

Raw proteomics data (XLSX)

Proteomic sample key (XLSX)

Details about instruments, materials, methods, chemical synthesis, ^{1}H and ^{31}P NMR characterization, LC–MS characterization, and Western Blots (PDF)

Accession Codes

Accession Codes CCDC 2480193–2480194; the supplementary crystallographic data for this paper. These data can be obtained free of charge via www.ccdc.cam.ac.uk/data_request/cif, or by emailing data_request@ccdc.cam.ac.uk, or by contacting The Cambridge Crystallographic Data Centre, 12 Union Road, Cambridge CB2 1EZ, UK; fax: + 44 1223 336033.

■ AUTHOR INFORMATION

Corresponding Author

Samuel G. Awuah − *Department of Chemistry, University of Kentucky, Lexington, Kentucky 40506, United States; Center for Pharmaceutical Research and Innovation, Department of Pharmaceutical Sciences, College of Pharmacy and Markey NCI Comprehensive Cancer Center, University of Kentucky, Lexington, Kentucky 40536, United States; University of Kentucky Bioelectronics and Nanomedicine Research Center, Lexington, Kentucky 40506, United States;* orcid.org/0000-0003-4947-7283; Email: awuah@uky.edu

Authors

Sean T. Gilpatrick − *Department of Chemistry, University of Kentucky, Lexington, Kentucky 40506, United States*

Jong Hyun Kim − *Department of Chemistry, University of Kentucky, Lexington, Kentucky 40506, United States*

Sarayu Bhogoju − *Department of Medicine, Division of Digestive Diseases and Nutrition, University of Kentucky College of Medicine, Lexington, Kentucky 40506, United States; Lexington Veterans Affairs Medical Center Kentucky, Lexington, Kentucky 40506, United States*

Neeraj Kapur − *Department of Medicine, Division of Digestive Diseases and Nutrition, University of Kentucky College of Medicine, Lexington, Kentucky 40506, United States; Lexington Veterans Affairs Medical Center Kentucky, Lexington, Kentucky 40506, United States*

Udara Munugoda − *Department of Chemistry, University of Kentucky, Lexington, Kentucky 40506, United States*

Jovita Daraezinwa − *Department of Chemistry, University of Kentucky, Lexington, Kentucky 40506, United States*

Sean Parkin − *Department of Chemistry, University of Kentucky, Lexington, Kentucky 40506, United States*

Terrence A. Barrett − *Department of Medicine, Division of Digestive Diseases and Nutrition, University of Kentucky College of Medicine, Lexington, Kentucky 40506, United States; Lexington Veterans Affairs Medical Center Kentucky, Lexington, Kentucky 40506, United States*

Christine F. Brainson − *Department of Toxicology and Cancer Biology and Center for Pharmaceutical Research and Innovation, Department of Pharmaceutical Sciences, College of Pharmacy, University of Kentucky, Lexington, Kentucky 40536, United States;* orcid.org/0000-0002-0854-5043

Daniel R. Plaugher − *Department of Toxicology and Cancer Biology, University of Kentucky, Lexington, Kentucky 40536, United States*

Complete contact information is available at: https://pubs.acs.org/10.1021/jacs.6c00003

Notes

The authors declare the following competing financial interest(s): Samuel G. Awuah has patents pending to University of Kentucky Research Foundation.

■ ACKNOWLEDGMENTS

This work and S.G.A. were supported by grant R01CA258421-01 from the National Cancer Institute. S.G.A. acknowledges support by KSCHIRT, P20GM130456, and Mid-South REACH grants. Support for T. B. by VA Merit awards I01BX006870-01 and 5I01CX001353, NIH-NIDDK (R01) 5R01DK095662-12 is acknowledged. D.R.P. acknowledges support by NCI K99CA303792. C.F.B. acknowledges support by NCI R01-HL170193. We gratefully acknowledge the support of various facilities at the University of Kentucky, including the UK NMR Center (NSF-CHE-997738), the UK X-ray facility (NSF-CHE-1625732), and the Redox Metabolism Shared Resource of the University of Kentucky Markey Cancer Center (P30CA177558). We also appreciate the assistance of Dr. Andrew Lemoff and the Proteomics Core facility at UT Southwestern for mass spectrometry and proteomics expertise.

■ REFERENCES

(1) Nishida, N. Role of Oncogenic Pathways on the Cancer Immunosuppressive Microenvironment and Its Clinical Implications in Hepatocellular Carcinoma. *Cancers* **2021**, *13* (15), 3666.

(2) Fitzsimmons, T. S.; Singh, N.; Walker, T. D. J.; Newton, C.; Evans, D. G. R.; Crosbie, E. J.; Ryan, N. A. J. Immune checkpoint inhibitors efficacy across solid cancers and the utility of PD-L1 as a biomarker of response: a systematic review and meta-analysis. *Front. Med.* **2023**, *10*, 1192762.

(3) (a) Jiang, Q.; Zhang, C.; Wang, H.; Peng, T.; Zhang, L.; Wang, Y.; Han, W.; Shi, C. Mitochondria-Targeting Immunogenic Cell Death Inducer Improves the Adoptive T-Cell Therapy Against Solid Tumor. *Front. Oncol.* **2019**, *9*, 1196. (b) Zhao, H.-Y.; Li, K.-H.; Wang, D.-D.; Zhang, Z.-L.; Xu, Z.-J.; Qi, M.-H.; Huang, S.-W. A mitochondria-targeting dihydroartemisinin derivative as a reactive oxygen species -based immunogenic cell death inducer. *iScience* **2024**, *27* (1), 108702.
(4) Messina, A.; Reina, S.; Guarino, F.; De Pinto, V. VDAC isoforms in mammals. *Biochim. Biophys. Acta* **2012**, *1818* (6), 1466−1476.
(5) Shoshan-Barmatz, V.; N Maldonado, E.; Krelin, Y. VDAC1 at the crossroads of cell metabolism, apoptosis and cell stress. *Cell Stress* **2017**, *1* (1), 11−36.
(6) (a) Shoshan-Barmatz, V.; Ben-Hail, D.; Admoni, L.; Krelin, Y.; Tripathi, S. S. The mitochondrial voltage-dependent anion channel 1 in tumor cells. *Biochim. Biophys. Acta* **2015**, *1848* (10), 2547−2575. (b) Conti Nibali, S.; De Siervi, S.; Luchinat, E.; Magrì, A.; Messina, A.; Brocca, L.; Mantovani, S.; Oliviero, B.; Ahmed, M. H.; Mondelli, M. U.; et al. VDAC1-interacting molecules promote cell death in cancer organoids through mitochondrial-dependent metabolic interference. *iScience* **2024**, *27* (6), 109853. (c) Wang, Z.; Cheng, Y.; Song, Z.; Zhao, R. Pan-Cancer Analysis of Voltage-Dependent Anion Channel (VDAC1) as a Cancer Therapeutic Target or Diagnostic Biomarker. *Dis. Markers* **2022**, *2022*, 1−19.
(7) (a) Manczak, M.; Reddy, P. H. Abnormal interaction of VDAC1 with amyloid beta and phosphorylated tau causes mitochondrial dysfunction in Alzheimer's disease. *Hum. Mol. Genet.* **2012**, *21* (23), 5131−5146. (b) Cavallaro, F.; Conti Nibali, S.; Cubisino, S. A. M.; Caruso, P.; Zimbone, S.; Infantino, I. R.; Reina, S.; De Pinto, V.; Messina, A.; Giuffrida, M. L.; Magrì, A. VDAC1-Targeted NHK1 Peptide Recovers Mitochondrial Dysfunction Counteracting Amyloid-β Oligomers Toxicity in Alzheimer's Disease. *Aging Cell* **2025**, *24* (7), No. e70069.
(8) Ma, Y.; Sun, X.; Yao, X. The role and mechanism of VDAC1 in type 2 diabetes: An underestimated target of environmental pollutants. *Mitochondrion* **2024**, *78*, 101929.
(9) Lin, D.; Cui, B.; Ren, J.; Ma, J. Regulation of VDAC1 contributes to the cardioprotective effects of penehyclidine hydrochloride during myocardial ischemia/reperfusion. *Exp. Cell Res.* **2018**, *367* (2), 257−263.
(10) Yagoda, N.; von Rechenberg, M.; Zaganjor, E.; Bauer, A. J.; Yang, W. S.; Fridman, D. J.; Wolpaw, A. J.; Smukste, I.; Peltier, J. M.; Boniface, J. J.; et al. RAS−RAF−MEK-dependent oxidative cell death involving voltage-dependent anion channels. *Nature* **2007**, *447* (7146), 865−869.
(11) (a) Israelson, A.; Arzoine, L.; Abu-hamad, S.; Khodorkovsky, V.; Shoshan-Barmatz, V. A Photoactivable Probe for Calcium Binding Proteins. *Chem. Biol.* **2005**, *12* (11), 1169−1178. (b) Israelson, A.; Zaid, H.; Abu-Hamad, S.; Nahon, E.; Shoshan-Barmatz, V. Mapping the ruthenium red-binding site of the voltage-dependent anion channel-1. *Cell Calcium* **2008**, *43* (2), 196−204.
(12) Ben-Hail, D.; Begas-Shvartz, R.; Shalev, M.; Shteinfer-Kuzmine, A.; Gruzman, A.; Reina, S.; De Pinto, V.; Shoshan-Barmatz, V. Novel Compounds Targeting the Mitochondrial Protein VDAC1 Inhibit Apoptosis and Protect against Mitochondrial Dysfunction. *J. Biol. Chem.* **2016**, *291* (48), 24986−25003.
(13) Verma, A.; Shteinfer-Kuzmine, A.; Kamenetsky, N.; Pittala, S.; Paul, A.; Nahon Crystal, E.; Ouro, A.; Chalifa-Caspi, V.; Pandey, S. K.; Monsonego, A.; et al. Targeting the overexpressed mitochondrial protein VDAC1 in a mouse model of Alzheimer's disease protects against mitochondrial dysfunction and mitigates brain pathology. *Transl. Neurodegener.* **2022**, *11* (1), 58.
(14) Zhang, E.; Mohammed Al-Amily, I.; Mohammed, S.; Luan, C.; Asplund, O.; Ahmed, M.; Ye, Y.; Ben-Hail, D.; Soni, A.; Vishnu, N.; et al. Preserving Insulin Secretion in Diabetes by Inhibiting VDAC1 Overexpression and Surface Translocation in β Cells. *Cell Metab.* **2019**, *29* (1), 64−77.
(15) Kim, J.; Gupta, R.; Blanco, L. P.; Yang, S.; Shteinfer-Kuzmine, A.; Wang, K.; Zhu, J.; Yoon, H. E.; Wang, X.; Kerkhofs, M.; et al. VDAC oligomers form mitochondrial pores to release mtDNA fragments and promote lupus-like disease. *Science* **2019**, *366* (6472), 1531−1536.
(16) Verma, A.; Pittala, S.; Alhozeel, B.; Shteinfer-Kuzmine, A.; Ohana, E.; Gupta, R.; Chung, J. H.; Shoshan-Barmatz, V. The role of the mitochondrial protein VDAC1 in inflammatory bowel disease: a potential therapeutic target. *Mol. Ther.* **2022**, *30* (2), 726−744.
(17) Mertens, R. T.; Gukathasan, S.; Arojojoye, A. S.; Olelewe, C.; Awuah, S. G. Next Generation Gold Drugs and Probes: Chemistry and Biomedical Applications. *Chem. Rev.* **2023**, *123* (10), 6612−6667.
(18) Finkelstein, A. E.; Walz, D. T.; Batista, V.; Mizraji, M.; Roisman, F.; Misher, A. A. New oral gold compound for treatment of rheumatoid arthritis. *Ann. Rheum. Dis.* **1976**, *35* (3), 251−257.
(19) (a) Jahid, M.; Khan, K. U.; Rehan Ul, H.; Ahmed, R. S. Overview of Rheumatoid Arthritis and Scientific Understanding of the Disease. *Mediterr J. Rheumatol.* **2023**, *34* (3), 284−291. (b) Forestier, J. The treatment of rheumatoid arthritis with gold salts injections. *Lancet* **1932**, *219* (5661), 441−444.
(20) Furst, D. E. Mechanism of Action, Pharmacology, Clinical Efficacy and Side Effects of Auranofin: An Orally Administered Organic Gold Compound for the Treatment of Rheumatoid Arthritis. Pharmacotherapy. *J. Human Pharmacol. Drug Therapy* **1983**, *3* (5), 284−296.
(21) Youn, H. S.; Lee, J. Y.; Saitoh, S. I.; Miyake, K.; Hwang, D. H. A. as an anti-rheumatic gold compound, suppresses LPS-induced homodimerization of TLR4. *Biochem. Biophys. Res. Commun.* **2006**, *350* (4), 866−871.
(22) Hwangbo, H.; Ji, S. Y.; Kim, M. Y.; Kim, S. Y.; Lee, H.; Kim, G.-Y.; Kim, S.; Cheong, J.; Choi, Y. H. Anti-Inflammatory Effect of Auranofin on Palmitic Acid and LPS-Induced Inflammatory Response by Modulating TLR4 and NOX4-Mediated NF-κB Signaling Pathway in RAW264.7 Macrophages. *Int. J. Mol. Sci.* **2021**, *22* (11), 5920.
(23) (a) Mertens, R. T.; Parkin, S.; Awuah, S. G. Cancer cell-selective modulation of mitochondrial respiration and metabolism by potent organogold(III) dithiocarbamates. *Chem. Sci.* **2020**, *11* (38), 10465−10482. (b) Hyun Kim, J.; Ofori, S.; Mertens, R. T.; Parkin, S.; Awuah, S. G. Water-Soluble Gold(III)−Metformin Complex Alters Mitochondrial Bioenergetics in Breast Cancer Cells. *ChemMedChem* **2021**, *16* (20), 3222−3230. (c) Arojojoye, A. S.; Olelewe, C.; Gukathasan, S.; Kim, J. H.; Vekaria, H.; Parkin, S.; Sullivan, P. G.; Awuah, S. G. Serum-Stable Gold(III) Bisphosphine Complex Induces Mild Mitochondrial Uncoupling and In Vivo Antitumor Potency in Triple Negative Breast Cancer. *J. Med. Chem.* **2023**, *66* (12), 7868−7879. (d) Gilpatrick, S. T.; Obisesan, O. A.; Parkin, S.; Awuah, S. G. Carbon−phosphorus stapled Au(I) anticancer agents via bisphosphine induced reductive elimination. *Dalton Trans.* **2024**, *53* (47), 18974−18982. (e) Olelewe, C.; Awuah, S. G. Mitochondria as a target of third row transition metal-based anticancer complexes. *Curr. Opin. Chem. Biol.* **2023**, *72*, 102235.
(24) Sen, S.; Hufnagel, S.; Maier, E. Y.; Aguilar, I.; Selvakumar, J.; DeVore, J. E.; Lynch, V. M.; Arumugam, K.; Cui, Z.; Sessler, J. L.; Arambula, J. F. Rationally Designed Redox-Active Au(I) N-Heterocyclic Carbene: An Immunogenic Cell Death Inducer. *J. Am. Chem. Soc.* **2020**, *142* (49), 20536−20541.
(25) Huang, K.-B.; Wang, F.-Y.; Tang, X.-M.; Feng, H.-W.; Chen, Z.-F.; Liu, Y.-C.; Liu, Y.-N.; Liang, H. Organometallic Gold(III) Complexes Similar to Tetrahydroisoquinoline Induce ER-Stress-Mediated Apoptosis and Pro-Death Autophagy in A549 Cancer Cells. *J. Med. Chem.* **2018**, *61* (8), 3478−3490.
(26) (a) Tomasello, M. F.; Nardon, C.; Lanza, V.; Di Natale, G.; Pettenuzzo, N.; Salmaso, S.; Milardi, D.; Caliceti, P.; Pappalardo, G.; Fregona, D. New comprehensive studies of a gold(III) Dithiocarbamate complex with proven anticancer properties: Aqueous dissolution with cyclodextrins, pharmacokinetics and upstream inhibition of the ubiquitin-proteasome pathway. *Eur. J. Med. Chem.* **2017**, *138*, 115−127. (b) Lipiec, S.; Gurba, A.; Agnieszczak, I. M.; Szczepankiewicz, A. A.; Szymański, P.; Taciak, P.; Szczepaniak, R.; Szeleszczuk, Ł.; Nieznanska, H.; Włodarczyk, J.; et al. New gold(III) cyanide complex TGS 121 induces ER stress, proteasome inhibition and death of Ras-hyperactivated cells. *Toxicol. In Vitro* **2023**, *88*, 105556.

https://doi.org/10.1021/jacs.6c00003
J. Am. Chem. Soc. XXXX, XXX, XXX−XXX

(27) Kim, J. H.; Ofori, S.; Parkin, S.; Vekaria, H.; Sullivan, P. G.; Awuah, S. G. Anticancer gold(III)-bisphosphine complex alters the mitochondrial electron transport chain to induce in vivo tumor inhibition. *Chem. Sci.* **2021**, *12* (21), 7467−7479.
(28) Mármol, I.; Virumbrales-Muñoz, M.; Quero, J.; Sánchez-de-Diego, C.; Fernández, L.; Ochoa, I.; Cerrada, E.; Yoldi, M. J. R. Alkynyl gold(I) complex triggers necroptosis via ROS generation in colorectal carcinoma cells. *J. Inorg. Biochem.* **2017**, *176*, 123−133.
(29) Cheng, X.; Haeberle, S.; Shytaj, I. L.; Gama-Brambila, R. A.; Theobald, J.; Ghafoory, S.; Wölker, J.; Basu, U.; Schmidt, C.; Timm, A.; et al. NHC-gold compounds mediate immune suppression through induction of AHR-TGFβ1 signalling in vitro and in scurfy mice. *Commun. Biol.* **2020**, *3* (1), 10.
(30) Levine, M. S.; Sen, S.; Maier, E. Y.; Mota, M.; Won, M.; Li, J.; Arambula, J. F.; Lynch, V. M.; Kim, J. S.; DePinho, R. A.; et al. Long-Lived Immunogenic Cell Death Induced by a Water-Soluble Redox Active Au(I) Bis-N-Heterocyclic Carbene. *J. Am. Chem. Soc.* **2025**, *147* (27), 23574−23582.
(31) (a) Giorgio, A.; Merlino, A. Gold metalation of proteins: Structural studies. *Coord. Chem. Rev.* **2020**, *407*, 213175. (b) Bhabak, K. P.; Bhuyan, B. J.; Mugesh, G. Bioinorganic and medicinal chemistry: aspects of gold(i)-protein complexes. *Dalton Trans.* **2011**, *40* (10), 2099−2111.
(32) Messori, L.; Abbate, F.; Marcon, G.; Orioli, P.; Fontani, M.; Mini, E.; Mazzei, T.; Carotti, S.; O'Connell, T.; Zanello, P. Gold(III) Complexes as Potential Antitumor Agents: Solution Chemistry and Cytotoxic Properties of Some Selected Gold(III) Compounds. *J. Med. Chem.* **2000**, *43* (19), 3541−3548.
(33) Gukathasan, S.; Parkin, S.; Black, E. P.; Awuah, S. G. Tuning Cyclometalated Gold(III) for Cysteine Arylation and Ligand-Directed Bioconjugation. *Inorg. Chem.* **2021**, *60* (19), 14582−14593.
(34) Munugoda, U.; Gilpatrick, S. T.; Das, D.; Parkin, S.; Miller, A.-F.; Awuah, S. G. Cyclometalated Gold(III)-Mediated Cysteine Arylation: A Bioorthogonal Platform for Covalent Targeting of Intrinsically Disordered Proteins. *Angew. Chem. Int. Ed.* **2025**, *64* (50), No. e202516331.
(35) (a) Wenzel, M.; Casini, A. Mass spectrometry as a powerful tool to study therapeutic metallodrugs speciation mechanisms: Current frontiers and perspectives. *Coord. Chem. Rev.* **2017**, *352*, 432−460. (b) Wang, H.; Zhou, Y.; Xu, X.; Li, H.; Sun, H. Metalloproteomics in conjunction with other omics for uncovering the mechanism of action of metallodrugs: Mechanism-driven new therapy development. *Curr. Opin. Chem. Biol.* **2020**, *55*, 171−179.
(36) Babak, M. V.; Meier, S. M.; Huber, K. V. M.; Reynisson, J.; Legin, A. A.; Jakupec, M. A.; Roller, A.; Stukalov, A.; Gridling, M.; Bennett, K. L.; et al. Target profiling of an antimetastatic RAPTA agent by chemical proteomics: relevance to the mode of action. *Chem. Sci.* **2015**, *6* (4), 2449−2456.
(37) Hu, D.; Liu, Y.; Lai, Y.-T.; Tong, K.-C.; Fung, Y.-M.; Lok, C.-N.; Che, C.-M. Anticancer Gold(III) Porphyrins Target Mitochondrial Chaperone Hsp60. *Angew. Chem. Int. Ed.* **2016**, *55* (4), 1387−1391.
(38) Gukathasan, S.; Olelewe, C.; Ratliff, L.; Kim, J. H.; Ackerman, A. M.; McCorkle, J. R.; Parkin, S.; Kwakye, G. F.; Kolesar, J. M.; Awuah, S. G. Chemoproteomic Profiling of a Carbon-Stabilized Gold(III) Macrocycle Reveals Cellular Engagement with HMOX2. *J. Med. Chem.* **2025**, *68* (5), 5687−5698.
(39) Arojojoye, A. S.; Awuah, S. G. Functional utility of gold complexes with phosphorus donor ligands in biological systems. *Coord. Chem. Rev.* **2025**, *522*, 216208.
(40) Shoemaker, R. H. The NCI60 human tumour cell line anticancer drug screen. *Nat. Rev. Cancer* **2006**, *6* (10), 813−823.
(41) Reinhold, W. C.; Sunshine, M.; Liu, H.; Varma, S.; Kohn, K. W.; Morris, J.; Doroshow, J.; Pommier, Y. CellMiner: A Web-Based Suite of Genomic and Pharmacologic Tools to Explore Transcript and Drug Patterns in the NCI-60 Cell Line Set. *Cancer Res.* **2012**, *72* (14), 3499−3511.
(42) Moyer, M. P.; Manzano, L. A.; Merriman, R. L.; Stauffer, J. S.; Tanzer, L. R. NCM-460, a normal human colon mucosal epithelial cell line. *In Vitro Cell. Dev. Biol.: Anim.* **1996**, *32* (6), 315−317.
(43) Du, H.; Xu, T.; Yu, S.; Wu, S.; Zhang, J. Mitochondrial metabolism and cancer therapeutic innovation. *Signal Transduction Targeted Ther.* **2025**, *10* (1), 245.
(44) (a) Pu, X.; Zhang, Q.; Liu, J.; Wang, Y.; Guan, X.; Wu, Q.; Liu, Z.; Liu, R.; Chang, X. Ginsenoside Rb1 ameliorates heart failure through DUSP-1-TMBIM-6-mediated mitochondrial quality control and gut flora interactions. *Phytomedicine* **2024**, *132*, 155880. (b) Lu, C.; Yang, B.; Liu, Y.; Liu, W.; Yan, J.; Guo, C.; Song, T.; Wang, X. Carvacrol Regulates the Expression of SLC25A6 by Inhibiting VDAC1 to Improve Mitochondrial Function and Reduce LPS-Induced Inflammatory Injury in HMEC-1 Cells. *ACS Omega* **2025**, *10* (8), 8512−8522. (c) Yuan, S.; Sun, R.; Shi, H.; Chapman, N. M.; Hu, H.; Guy, C.; Rankin, S.; Kc, A.; Palacios, G.; Meng, X.; et al. VDAC2 loss elicits tumour destruction and inflammation for cancer therapy. *Nature* **2025**, *640* (8060), 1062−1071. (d) Argueti-Ostrovsky, S.; Barel, S.; Kahn, J.; Israelson, A. VDAC1: A Key Player in the Mitochondrial Landscape of Neurodegeneration. *Biomolecules* **2025**, *15* (1), 33. (e) Lafargue, E.; Duneau, J.-P.; Buzhinsky, N.; Ornelas, P.; Ortega, A.; Ravishankar, V.; Sturgis, J.; Casuso, I.; Bergdoll, L. Membrane lipid composition modulates the organization of VDAC1, a mitochondrial gatekeeper. *Commun. Biol.* **2025**, *8* (1), 936.
(45) (a) Zhou, R.; Yazdi, A. S.; Menu, P.; Tschopp, J. A role for mitochondria in NLRP3 inflammasome activation. *Nature* **2011**, *469* (7329), 221−225. (b) Xian, H.; Watari, K.; Sanchez-Lopez, E.; Offenberger, J.; Onyuru, J.; Sampath, H.; Ying, W.; Hoffman, H. M.; Shadel, G. S.; Karin, M. Oxidized DNA fragments exit mitochondria via mPTP- and VDAC-dependent channels to activate NLRP3 inflammasome and interferon signaling. *Immunity* **2022**, *55* (8), 1370−1385.
(46) (a) Phan, L. M.; Yeung, S. C.; Lee, M. H. Cancer metabolic reprogramming: importance, main features, and potentials for precise targeted anti-cancer therapies. *Cancer Biol. Med.* **2014**, *11* (1), 1−19. (b) Maldonado, E. N.; Patnaik, J.; Mullins, M. R.; Lemasters, J. J. Free tubulin modulates mitochondrial membrane potential in cancer cells. *Cancer Res.* **2010**, *70* (24), 10192−10201.
(47) (a) Lv, J.; Xu, W.; Jiang, P.; Yu, W.; Xue, H.; Hu, N.; Cao, Y.; Zhang, H.; Yin, C.; Gao, R. Mitochondrial DNA release via VDAC1 in keratinocytes: a key driver of innate immunity and vitiligo pathogenesis. *Cell Death Dis.* **2026**, *17* (1), 318. (b) Wiser, C.; Kim, B.; Vincent, J.; Ascano, M. Small molecule inhibition of human cGAS reduces total cGAMP output and cytokine expression in cells. *Sci. Rep.* **2020**, *10* (1), 7604.

https://doi.org/10.1021/jacs.6c00003
J. Am. Chem. Soc. XXXX, XXX, XXX−XXX